Supporting Information

Facile One-Pot Synthesis of Au–Pd Core–Shell Nanoparticles with Enhanced Catalytic Performance

Yufen Chen[1,2], Gustavo Madrigal[2,3], Claudio Cazorla[2,3,4], Bernat Mundet[5], Kapil Gupta[5], Asier Agrelo-Lestón[1,2]†, Marina Armengol-Profitós[6], Miquel Torras[1,2], Lluís Soler[1,2], Jordi Llorca[1,2]**

[1]Department of Chemical Engineering, Universitat Politècnica de Catalunya, EEBE, Eduard Maristany 10-14, 08019 Barcelona, Spain.

[2]Center for Research in Multiscale Science and Engineering, Universitat Politècnica de Catalunya, EEBE, Eduard Maristany 10-14, 08019 Barcelona, Spain.

[3]Department of Physics, Universitat Politècnica de Catalunya, EEBE, Eduard Maristany 10-14, 08019 Barcelona, Spain.

[4]Institució Catalana de Recerca i Estudis Avançats (ICREA), Passeig Lluís Companys 23, 08010 Barcelona, Spain.

[5]Catalan Institute of Nanoscience and Nanotechnology (ICN2), CSIC and BIST, Campus UAB, 08193 Bellaterra, Barcelona, Spain.

[6]ALBA Synchrotron Light Source, Carrer de La Llum 2-26, 08290 Cerdanyola del Vallès, Barcelona, Spain

Corresponding authors' email addresses: jordi.llorca@upc.edu, lluis.soler.turu@upc.edu

Table S1. Metal loading values determined by ICP-OES.

Sample	Before photoreaction		After photoreaction	
	Pd wt%	Au wt%	Pd wt%	Au wt%
Au/TiO_2-BM	n.a.	0.96±0.03	n.a.	0.97±0.03
$Au_{1.6}Pd_1/TiO_2$-BM	0.23±0.06	0.77±0.04	0.25±0.05	0.74±0.04
$Au_{0.5}Pd_1/TiO_2$-BM	0.53±0.05	0.49±0.05	0.52±0.04	0.51±0.04
$Au_{1.6}$-Pd_1TiO_2-BM	0.25±0.06	0.72±0.04	0.23±0.06	0.77±0.03
Pd_1-$Au_{1.6}TiO_2$-BM	0.22±0.06	0.78±0.03	0.25±0.06	0.76±0.04
$Au_{0.2}Pd_1/TiO_2$-BM	0.77±0.05	0.23±0.09	0.74±0.04	0.22±0.08
Pd/TiO_2-BM	0.97±0.04	n.a.	0.96±0.05	n.a.
$Au_{1.6}Pd_1/TiO_2$-BMC	0.23±0.06	0.73±0.04	0.27±0.06	0.74±0.04
$Au_{1.6}Pd_1/TiO_2$-IWI	0.26±0.08	0.76±0.06	0.23±0.07	0.74±0.04
$Au_{0.75wt\%}/TiO_2$ + $Pd_{0.25wt\%}/TiO_2$	0.27±0.07	0.78±0.06	0.28±0.06	0.73±0.07

Table S2. Summary of reported AuPd/TiO_2 photocatalysts for photocatalytic H_2 production.

Cocatalyst composition	**TiO_2**	**AuPd Structure**	**Preparation method**	**AuPd size (nm)**	**Light source**	**Reaction medium**	**mmol H_2 h^{-1} g^{-1}**	**Ref.**
$Au_{0.25}Pd_{0.75}$	TiO_2-P25	Core-shell	Sonochemical reduction	~4	Xenon lamp	5 M EtOH	17.5	1
$Au_{0.75}Pd_{0.25}$ (molar ratio)	TiO_2 nanofibers	Alloy	Electrospinning	~14	Solar simulator (100 mW cm^{-2})	2.7 M HCOOH	17.7	2
AuPd (0.3 wt%)	TiO_2 nanosheet	Alloy	Chemical reduction	~5	Xenon lamp (UV-visible)	25% mol MeOH	0.53	3
Au_9Pd_1 (molar ratio, 1 wt%)	TiO_2 -P25	Alloy	Chemical reduction	~2.5–3	Xenon Lamp $\lambda \geq 420$ nm	25% vol TEOA	2.33	4
AuPd	TiO_2 nanotube	Alloy	Electron-beam evaporator	~2–4	AM1.5G one sun illumination	10% vol TEOA	2.92	5
Pd_1Au_1 (molar ratio, 1 wt%)	TiO_2 -P25	Core-shell	Sol-immobilization	~4–5	UV light 4 x 10^{17} photons/s	25% vol glycerol	19.6	6

$Au_{1.6}Pd_1$ (molar ratio,	TiO_2-P90	Core-shell	One-pot ball-milling	~2–4	UV light 81.5 mW cm^{-2}	10% mol EtOH	26.2 (UV) 53.3	This work

Table S3. Parameters used for the deconvolution of the Au *4f* and Pd *3d* spectra.

	Baseline	Peaks	Peak position (eV)	Spin-orbit splitting (eV)	Peak shape	FWHM (eV)
Au *4f*	Shirley	Au^0 ($4f_{7/2}$)	83.4	3.65	GL (86)	1.2
		Au^{1+} ($4f_{7/2}$)	84.5	3.65	GL (30)	1.5
		Au^{3+} ($4f_{7/2}$)	85.8	3.65	GL (30)	1.8-2
Pd *3d*	Shirley	Pd^0 ($3d_{5/2}$)	334.9	5.25	A(0.32,0.33,0)GL(30)	1.45-1.55
		Pd^{2+} ($3d_{5/2}$)	336.0	5.25	GL (30)	1.5 -1.6
		Pd^{4+} ($3d_{5/2}$)	337.0	5.25	GL (30)	1.5 -1.6

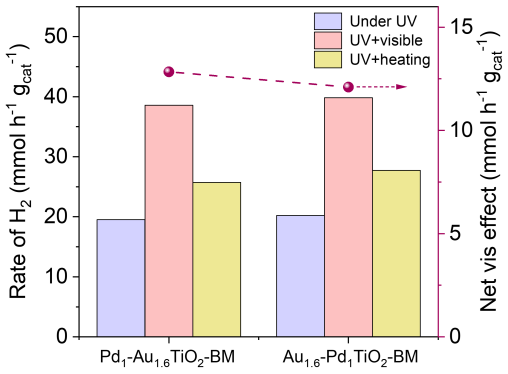


Figure S1. H_2 photoproduction rates of bimetallic cocatalyst supported-TiO_2 photocatalysts prepared by different milling orders.

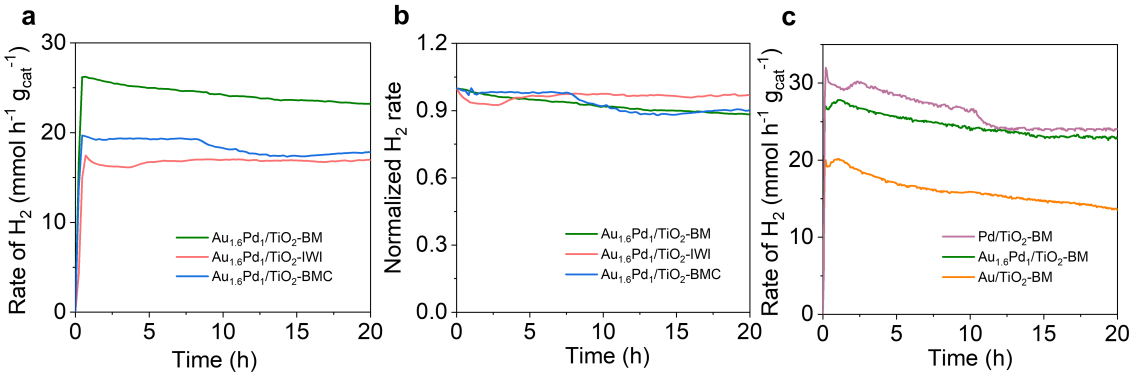


Figure S2. H_2 production rates in long-term stability tests under UV light irradiation of (a,b): $Au_{1.6}Pd_1/TiO_2$-BM, $Au_{1.6}Pd_1/TiO_2$-BMC and $Au_{1.6}Pd_1/TiO_2$-IWI, and (c): Pd/TiO_2-BM, $Au_{1.6}Pd_1/TiO_2$-BM and Au/TiO_2-BM.

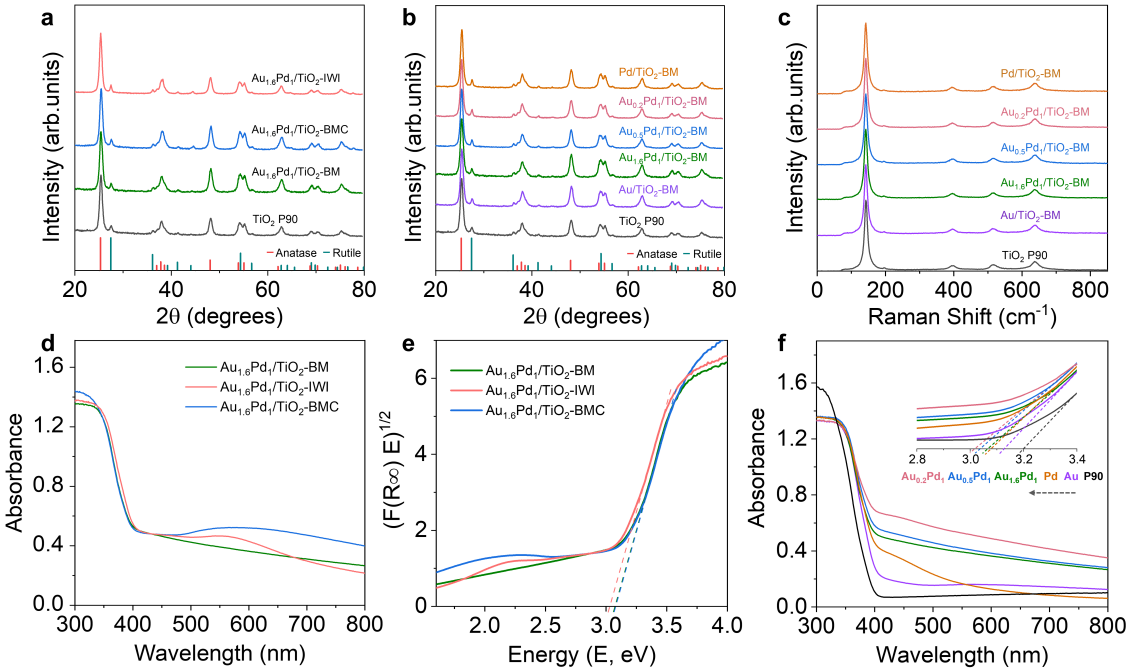


Figure S3. XRD patterns of (a) pristine TiO_2 P90 and $Au_{1.6}Pd_1/TiO_2$ samples prepared by BM, IWI and BMC methods, and (b) different Au/Pd ratio of Au_nPd_1/TiO_2-BM samples. (c) Raman spectra of Au_nPd_1/TiO_2-BM samples. (d-f) UV-vis absorption spectra and the corresponding Tauc plots of $(F(R_\infty)E)^{1/2}$ versus E (eV) for TiO_2, $Au_{1.6}Pd_1/TiO_2$-BM, $Au_{1.6}Pd_1/TiO_2$-IWI, $Au_{1.6}Pd_1/TiO_2$-BMC, and Au_nPd_1/TiO_2-BM samples. The dashed lines in (e) and (f) are a linear fit to determine the band gap energy (E_g) of photocatalysts.

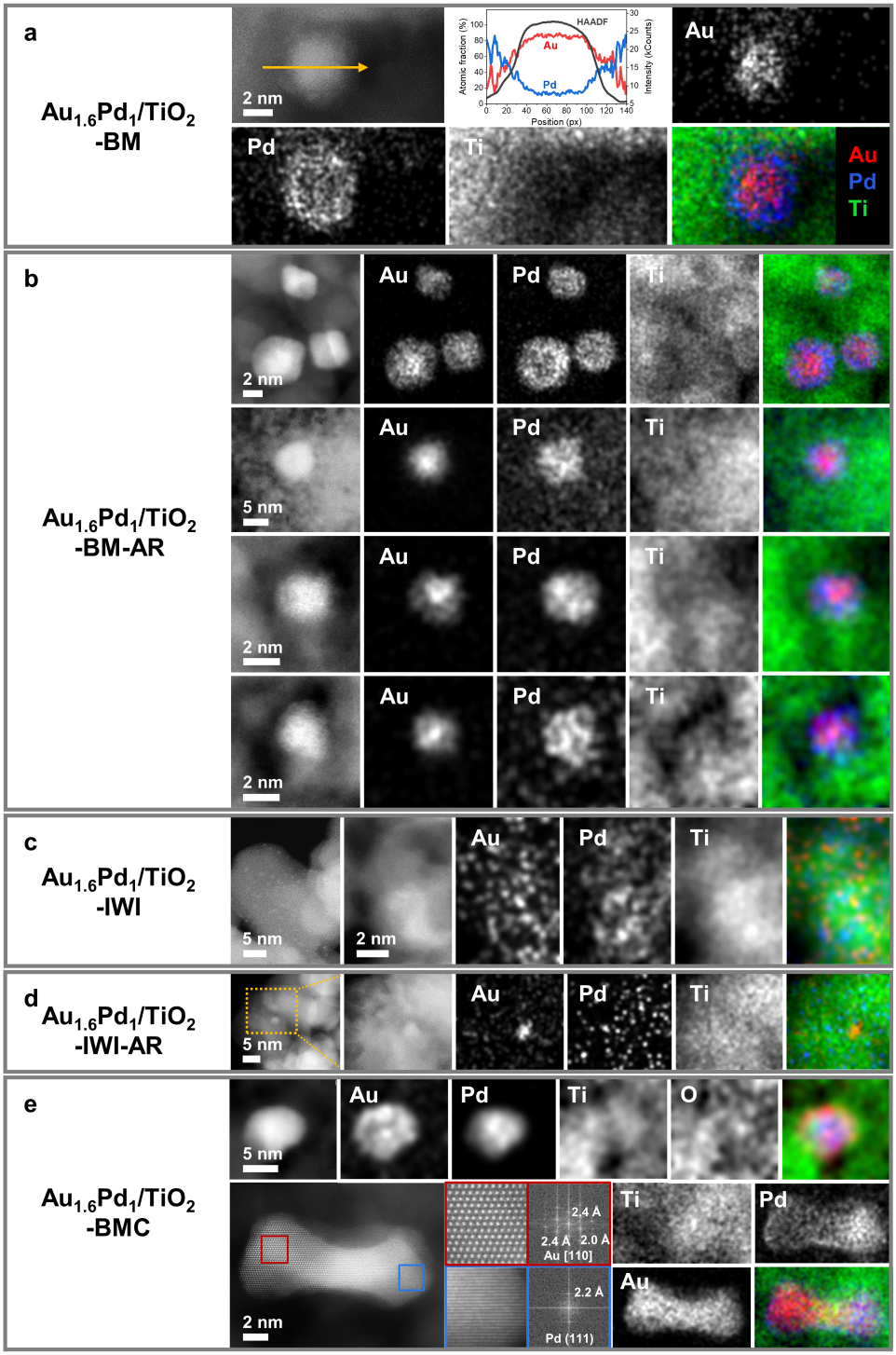


Figure S4. AC-HAADF-STEM images and corresponding elemental mappings of fresh and after reaction of $Au_{1.6}Pd_1/TiO_2$-BM (a,b) and $Au_{1.6}Pd_1/TiO_2$-IWI (c,d). AR refers to after reaction. (e), Fresh $Au_{1.6}Pd_1/TiO_2$-BMC. In all elemental mapping images, Au, Pd and Ti are represented in red, blue and green respectively. EDS line scan profiles of Au (red) and Pd (blue) in BM photocatalyst recorded along the arrow shown in (a). The red and blue frames in (e) present Fourier Transform (FT) images corresponding to the crystal planes of Au and Pd, respectively.

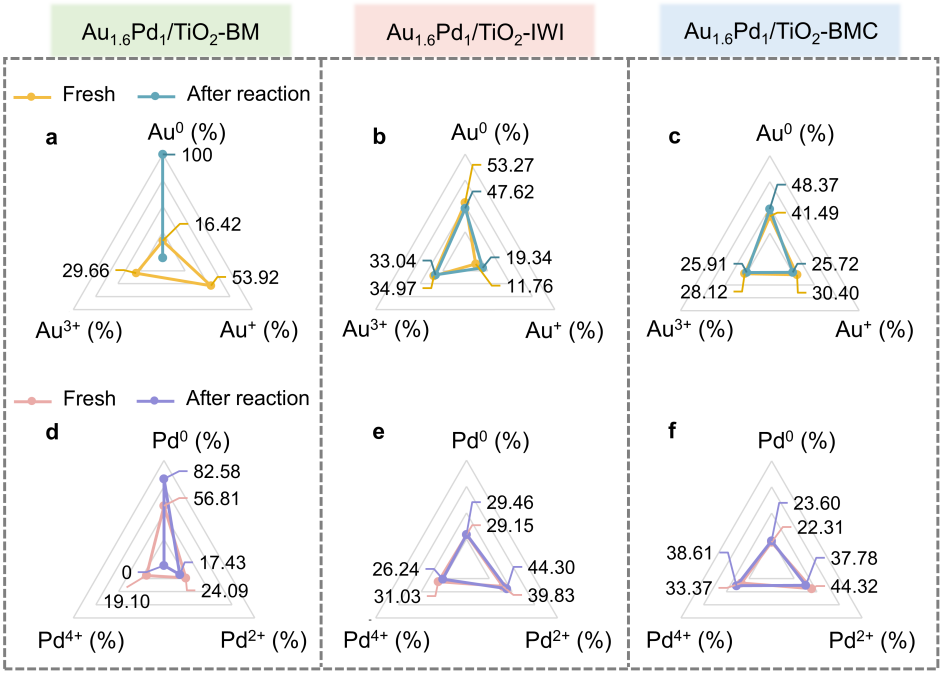


Figure S5. Corresponding ratios of Au and Pd oxidation states extracted from XP spectra in Fig. 3a-f.

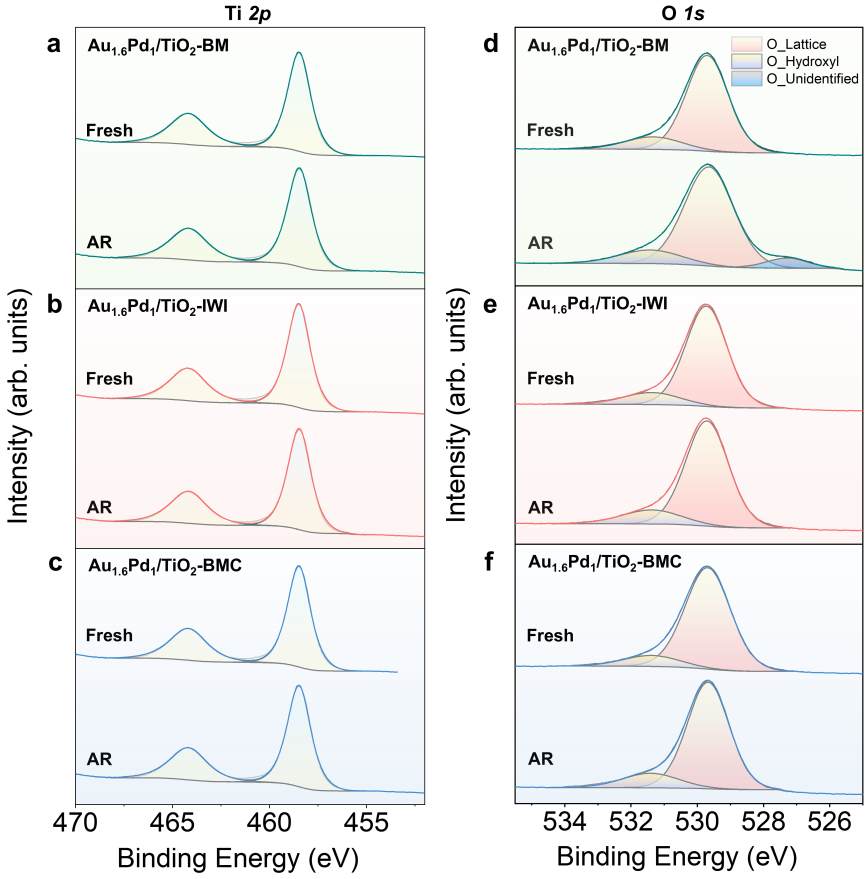


Figure S6. XP Ti *2p* (a, b, and c) and O *1s* (d, e, and f) spectra of fresh and after reaction of $Au_{1.6}Pd_1/TiO_2$-BM, $Au_{1.6}Pd_1/TiO_2$-IWI, and $Au_{1.6}Pd_1/TiO_2$-BMC photocatalysts. AR: after reaction.

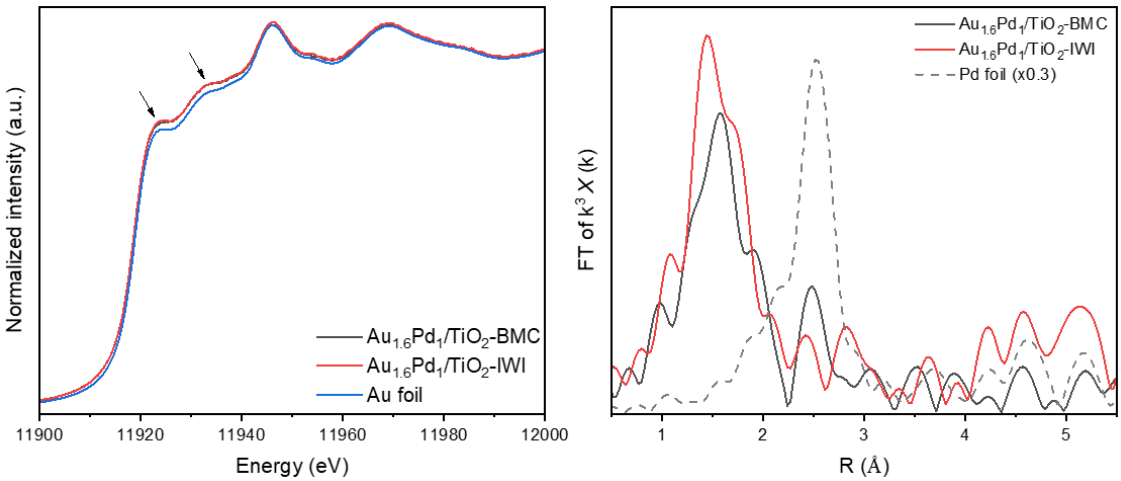


Figure S7. (a) Au L_3-edge XANES spectra of $Au_{1.6}Pd_1/TiO_2$-BMC, $Au_{1.6}Pd_1/TiO_2$-IWI, and Au foil as reference. (b) Pd K-edge EXAFS spectra in R-space (Fourier transform magnitude, phase-uncorrected) for $Au_{1.6}Pd_1/TiO_2$-BMC, $Au_{1.6}Pd_1/TiO_2$-IWI and Pd foil as reference.

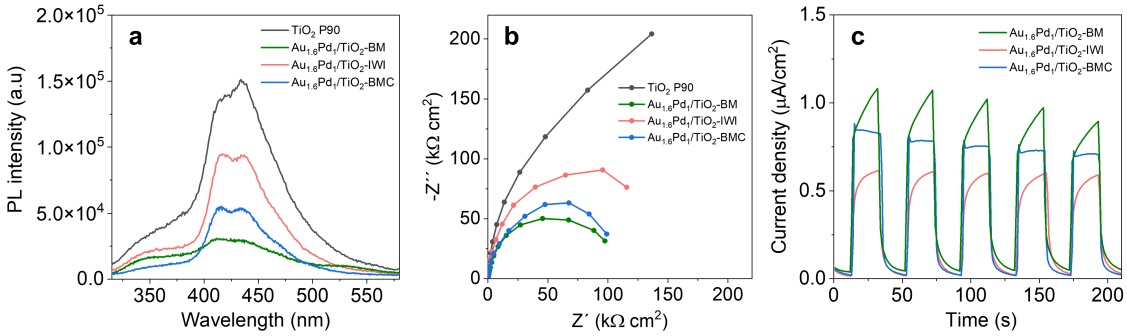


Figure S8. Photoluminescence (PL) spectra (a), EIS plots under solar simulator (b) and photocurrent response (c) of TiO_2, $Au_{1.6}Pd_1/TiO_2$-BM, $Au_{1.6}Pd_1/TiO_2$-IWI and $Au_{1.6}Pd_1/TiO_2$-BMC.

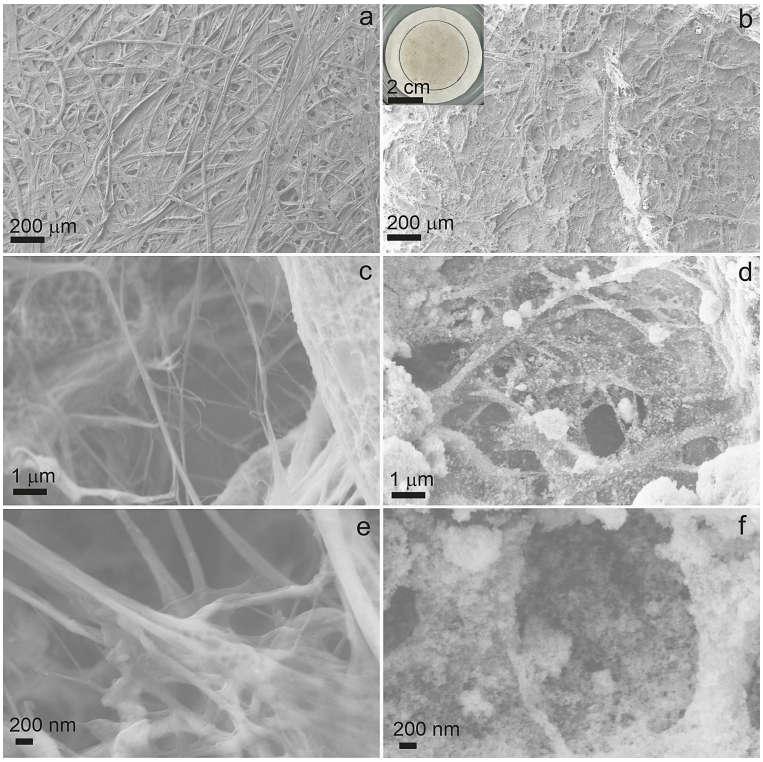


Figure S9. SEM micrographs at different magnifications of the cellulose paper used as a support to ensure the homogeneous distribution of the photocatalyst (a,c,e), and of the cellulose paper impregnated with the $Au_{1.6}Pd_1/TiO_2$-BM sample (b, d, f). The inset in panel b shows a photograph of the impregnated cellulose paper used in the photocatalytic experiments.

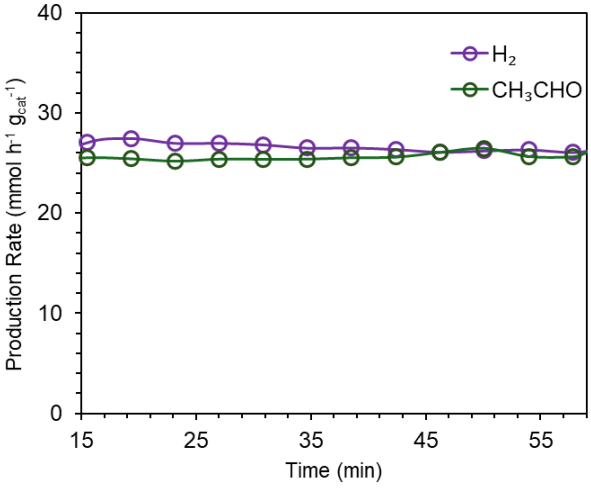


Figure S10. Time evolution of hydrogen and acetaldehyde photoproduction rates over AuPd/ TiO_2-BM under UV light. Hydrogen and acetaldehyde were the only detected products and were formed in equimolar amounts, confirming that ethanol dehydrogenation was the exclusive pathway for hydrogen production.

References

1. Mizukoshi, Y., Sato, K., Konno, T. J. & Masahashi, N. Dependence of photocatalytic activities upon the structures of Au/Pd bimetallic nanoparticles immobilized on TiO_2 surface. *Appl. Catal. B Environ.* **94**, 248–253 (2010).

2. Zhang, Z., Cao, S. W., Liao, Y. & Xue, C. Selective photocatalytic decomposition of formic acid over AuPd nanoparticle-decorated TiO_2 nanofibers toward high-yield hydrogen production. *Appl. Catal. B Environ.* **162**, 204–209 (2015).

3. Xin, Y. *et al.* Gold-palladium bimetallic nanoalloy decorated ultrathin 2D TiO_2 nanosheets as efficient photocatalysts with high hydrogen evolution activity. *J. Mater. Chem. A* **3**, 8659–8666 (2015).

4. Méndez-Medrano, A. A. *et al.* Enhanced Photocatalytic Activity of Surface-Modified TiO_2 with Bimetallic AuPd Nanoalloys for Hydrogen Generation. *Sol. RRL* **8**, 2400106 (2024).

5. Rajashekhar, H. *et al.* Bimetallic AuPd alloy nanoparticles on TiO_2 nanotube arrays: a highly efficient photocatalyst for hydrogen generation. *Nanotechnology* **36**, 205401 (2025).

6. Su, R. *et al.* Designer titania-supported Au-Pd nanoparticles for efficient photocatalytic hydrogen production. *ACS Nano* **8**, 3490–3497 (2014).